# Spex Young Star Atlas

We present a new spectral atlas of 46 young stars, compiled using a medium-resolution infrared spectrograph, SpeX, at the NASA Infrared Telescope Facility (IRTF) on Mauna Kea, Hawaii. SpeX maintains a resolution of $R \equiv \lambda/\Delta\lambda \sim 2000$, with a wavelength range of 0.70–2.55 $\mu$m. All atlas stars were selected from the star–forming region Upper Scorpius, which has a well-established age of ~11 Myr. Clear variations between old and young stars are observed, which will help constrain models of stellar evolution and atmospheres, at infrared wavelengths. Our new spectral atlas will allow for more accurate classification of young stars. Inconsistencies between infrared and optical spectral classifications will show the need for a more comprehensive young star library.

## 1. Introduction

Upper Scorpius (Upper Sco) is a star forming region located in the Scorpius-Centaurus Association. Members of star forming regions are born at approximately the same time. Upper Sco has an established age of ~11 Myr **?**. Old stars are currently used in identifying spectral type **??**. With ages on the order of billions of years, these stars do not accurately represent young stars.

Observations made of young stars exhibit unexpected spectral features. These variations prove young stars stars need independent spectral classification. A stellar atlas of young stars does not exist at infrared (IR) wavelengths. IR observations cut through gas and dust found in star forming regions.

Presented here is an atlas of young stars, allowing for more accurate classification. Criteria required in building such an atlas is discussed in Section 2.1. This atlas will allow for the refinement of stellar evolution and atmosphere models. Doing so will allow for more accurate spectral classification of young stars.

[young star - surface gravity?]
[why ir wavelength]
[future prospects]

## 2. Observations and Data Reduction

### 2.1. Sample Selection

We selected 46 members of the Upper Scorpius star forming region spanning spectral types from M–O. Prior to observation, each target was vetted using the following criteria. Stars identified to have binary companions **?** or accretion disks **?**, were eliminated from the target list. Restricting target objects based on such criteria ensures each observed spectra was as isolated and representative as possible.

To select potential targets, previously established spectral classes were used. Observations at optical wavelengths established spectral types, listed in Table 1.

## 2.2. Observations

All of the objects discussed in this paper were observed between March 2012 and June 2015 (Table 1), with the NASA Infra–Red Telescope Facility (IRTF) and the SpeX instrument **?**. We used the short–wavelength cross–dispersed mode (SXD) with $R2000$ matched to $0.3 \times 15$" slit. SpeX was upgraded in August 2014[1]. This upgrade increased the observable wavelength range, filled in the gap around $1.8\mu$m, and increased SpeX's wavelength sampling rate, allowing for higher accuracy of collected data. A portion of the objects in this catalog were observed prior to this upgrade. For this reason, it is necessary to compare data taken with each version of SpeX (Table 1), shown in Figure 2.

GSC 06801–00186 was observed on June 29, 2012 UT, before SpeX was upgraded, and again on June 15, 2015, after uSpeX was implemented **?**. Spectra collected after the upgrade span a larger wavelength range, but both SpeX and uSpeX data sufficiently cover the wavelength range needed for our study. Data collected with both versions follow the same procedure, discussed below. Before the upgrade, the wavelength range spanned 0.80–2.4 $\mu$m. Following August 2014, the wavelength range was expanded to span 0.70–2.55 $\mu$m.

During observations, integration times were altered as to maximize the Signal to Noise ratio (SNR). Observations were made in AB pairs. After the initial A frame is taken, the telescope offsets ("nods") and captures a B frame. Both frames are of the the same science target, at a different position along the slit. Since our objects were treated as point sources, this AB mode allowed for the subtraction of the B frame from the A frame, leaving both positive and negative spectrum along with sky residuals **?**. Subtraction of these pairs allows for the removal of dark currents and sky residuals.

After collecting data on a particular science object, flat and arc calibration frames were taken. In order to minimize the time between target observations and the collection of calibration frames, the telescope remained unmoved. Background noise was identified and removed using darks and flats.

Standard A0V stars also needed to be observed, for telluric line corrections. Which A0V to observe was determined by location and airmass. For our purposes, an ideal A0V would deviate from the science objects' airmass by no more than 0.15 and be located in the same region of the sky as the science object. This ensured minimal atmospheric derivations between our science and

---

[1]See `http://irtfweb.ifa.hawaii.edu/~spex/SpeX_manual_06mar15.pdf` for details.

A0V stars.

Effective temperatures with no identifying symbol come from from **?**. A least-squares fit to published values allowed for determination of temperatures for unlisted spectral types. Only values pertaining to specific luminosity classes were used in each fit.

## 2.3. Data Reduction

For reduction of collected spectra, Spextool was used **?**. Calibration frames consist of flats, arcs, and A0V standards. Flat frames allow for the removal of inconsistencies, amongst the detector's pixels. Observations of an arc lamp permitted wavelength calibration. The choice of A0V stars as standards was based on their relatively few spectral features, outside hydrogen lines; making isolation of telluric lines significantly cleaner. For telluric reduction, an observed A0V star was compared to Vega. Deviations of the observed star, from the standard, are attributed to atmospheric interference. The same atmospheric disturbances apply to all objects observed at the same time and airmass. Telluric corrections were accomplished using spectroscopic observations of standard stars. B–V data, provided by Simbad **?**, was used in in the standard selection process. In order to properly scale emission lines and account for velocity shifts, a kernel was constructed using the observed A0V. Finally, all orders were scaled and merged, producing a continuous spectrum. A more detailed account of this process is outlined by Vacca **?**.

To be transformed from an array into a workable spectrum Spextool **?** was used. Once extracted, each spectra was visually reviewed. Hot pixels, outliers, and areas of low SNR were masked and removed. Through this process, the intrinsic spectrum of each star was better revealed. SNR calculations occurred between 2.025–2.162 $\mu$m. All stars in this sample have SNR above 95.

## 3. Data and Analysis

### 3.1. The Spectra

[See commented-out list above]

Of the 46 stars composing this atlas, 9 have more than one spectral type referenced in the literature. For such stars, spectral classes referenced in Table 1 were determined by visual examination of individual spectra. Observed spectra were compared to existing libraries, with established spectral classes. References were chosen based on EW values and comparison of spectral features.

[**section 3.1 Rayner**]
[Digital copies of the spectra, with associated information, can be found at $----$.]

[Each spectra is available as a fits or png file.]
[Discuss masking of telluric regions.]

Table 2: EW Limit Definitions[2].

| Feature | Feature Limits ($\mu$m) | First Continuum Level Limits ($\mu$m) | Second Continuum Level Limit |
|---|---|---|---|
| Ca II (0.866 $\mu$m) | 0.8655–0.8673 | 0.862–0.864 | 0.870–0.873 |
| Na I (1.14 $\mu$m) | 1.137–1.1428 | 1.125–1.130 | 1.150–1.160 |
| Al I (1.313 $\mu$m) | 1.3118–1.3165 | 1.305–1.309 | 1.320–1.325 |
| Mg I (1.485 $\mu$m) | 1.4867–1.4895 | 1.4775–1.485 | 1.491–1.497 |
| Mg I (1.711 $\mu$m) | 1.7098–1.7130 | 1.702–1.708 | 1.715–1.720 |
| Na I (2.206 $\mu$m) | 2.204–2.211 | 2.192–2.198 | 2.213–2.220 |

### 3.2. Equivalent Widths

Following the procedure described by **?**, Equivalent width (EW) values and variances, $\sigma^2_{EW}$, are given by

$$EW = \sum_{i=1}^{n} \left[1 - \frac{f(\lambda_i)}{f_c(\lambda_i)}\right] \Delta\lambda_i, \tag{1}$$

$$\sigma^2_{EW} = \sum_{i=1}^{n} \Delta\lambda_i^2 \left[\frac{\sigma^2(\lambda_i)}{f_c^2(\lambda_i)} + \frac{f^2(\lambda_i)}{f_c^4(\lambda_i)}\sigma_c^2(\lambda_i)\right], \tag{2}$$

**C)**

where $f(\lambda_i)$ and $f_c(\lambda_i)$ are the observed and estimated continuum flux densities, respectively. Uncertainties in the observed and estimated continuum flux densities, $\sigma(\lambda_i)$ and $\sigma_c(\lambda_i)$, were calculated following the procedure of **?**. $\Delta\lambda$ is the difference between subsequent wavelength intervals; $\Delta\lambda = \lambda_{i+1} - \lambda_i$. To preserve dimensionality, $\lambda_n$ was appended to the end of each wavelength array, such that $\lambda_n = \lambda_{n+1}$.

Rather than subtracting adjacent intervals, **?** converted from wavelength to velocity–space and defined $d\nu = \nu_{i+\frac{1}{2}} - \nu_{i-\frac{1}{2}}$. Validation of these procedures was accomplished by calculating EW values and uncertainties of existing spectral libraries[3]. Calculated and published results were compared, showing both methodologies produce the same results.

---

[2] Table 8 of **?**.

[3] Table 9 of **?**.

**D)**

$$- - - - - - - - - --$$

where $f(\lambda_i)$ and $f_c(\lambda_i)$ are the observed and estimated continuum flux densities, respectively. Uncertainties in the observed and estimated continuum flux densities, $\sigma(\lambda_i)$ and $\sigma_c(\lambda_i)$, were calculated following the procedure of **?**. After converting from wavelength to velocity–space, **?** defined $d\nu = \nu_{i+\frac{1}{2}} - \nu_{i-\frac{1}{2}}$. Here, $\Delta\lambda$ is the difference between subsequent wavelength intervals; $\Delta\lambda = \lambda_{i+1} - \lambda_i$. To preserve dimensionality, $\lambda_n$ was appended to the end of each wavelength array, such that $\lambda_{n+1} = \lambda_n$. Validation of this procedure was accomplished by calculating $EW$ and $\sigma_{EW}$ for stars in existing spectral libraries[4]. Once calculated, results were compared to published values. Within error, both methods produce the same results.

$$- - - - - - - - - --$$

Spectral features act as indicators of many stellar properties. The absorption lines listed in Table 2 can be used to determine spectral types of cool stars **?**. Equivalent width (EW) values of these features are given in Table 3.

**Look at commented out lists above...and Discuss:**

- which lines were chosen and why

- how do the lines map to spt type...lum class

- what features are for young stars?

## 4. Comparison with Models

## 5. Needed Citations

**Sample Selection section**

- NEED NAME OF PERSON WHO COMPLETE BINART SURVEY - DAVID L (GEMINI)?

- NEED NAME OF PERSON WHO COMPLETED ACCRETION DISK SURVEY

**Observation section**

- ?

---

[4]Table 9 of **?**.

- cite whomever was referenced as identifying binaries **?**

- cite whomever was referenced as identifying accretion disks **?**

- when upgrade of Spex occurred **?**


- **?**


**Data Reduction and Analysis section**

- Lord, S. D., 1992, NASA Technical Memorandum 103957

- Gemini Observatory for telluric transmission regions shown in gray on plots

- Simbad


### 5.1.   From Adam Kraus

G, K, and early M stars: Kohler et al. (2000), Kraus et al. (2008), Lafreniere et al. (2014)

Mid/late M stars: Kraus et al. (2005), Bouy et al. (2006), Biller et al. (2011), Kraus & Hillenbrand (2012)

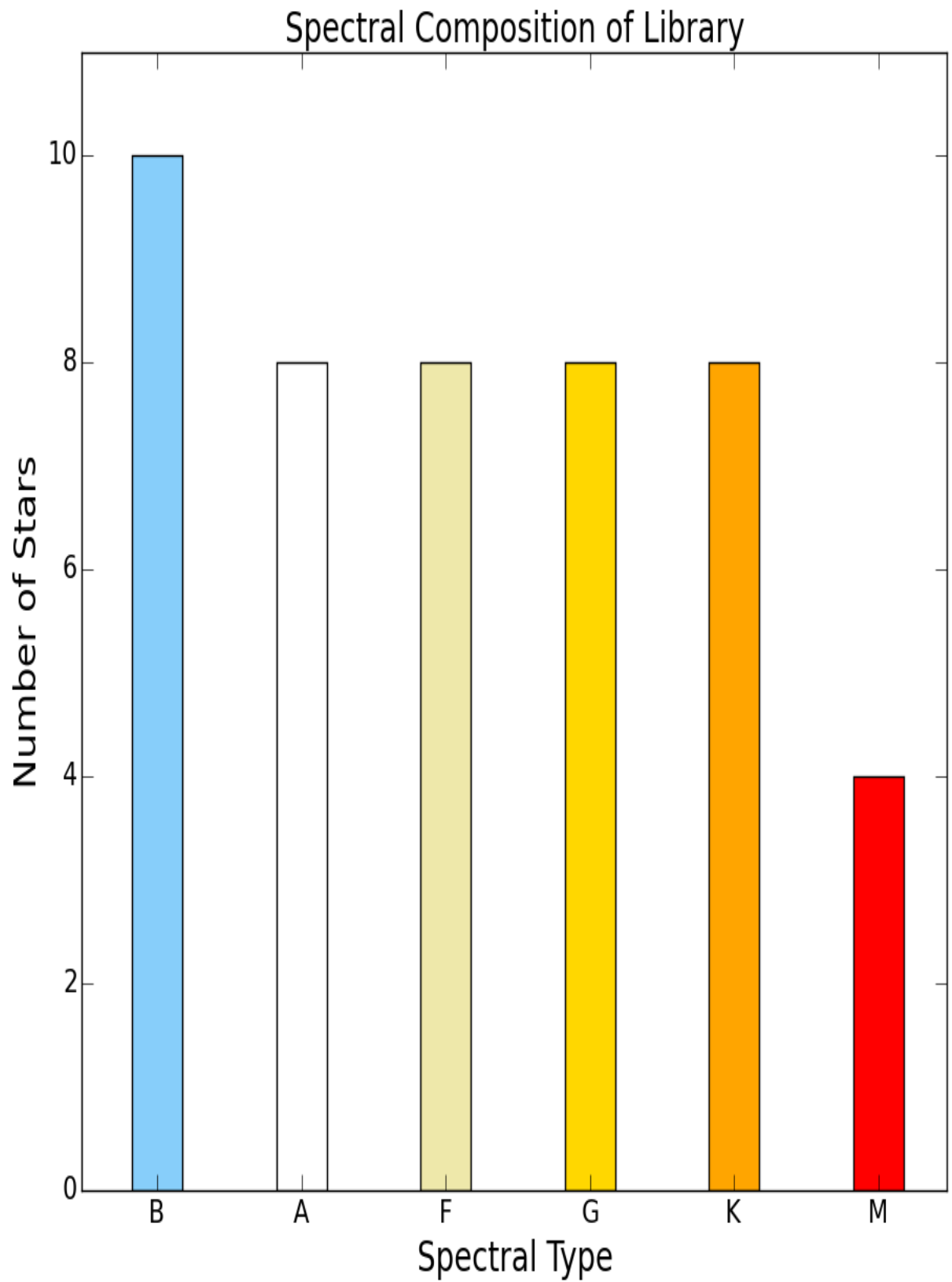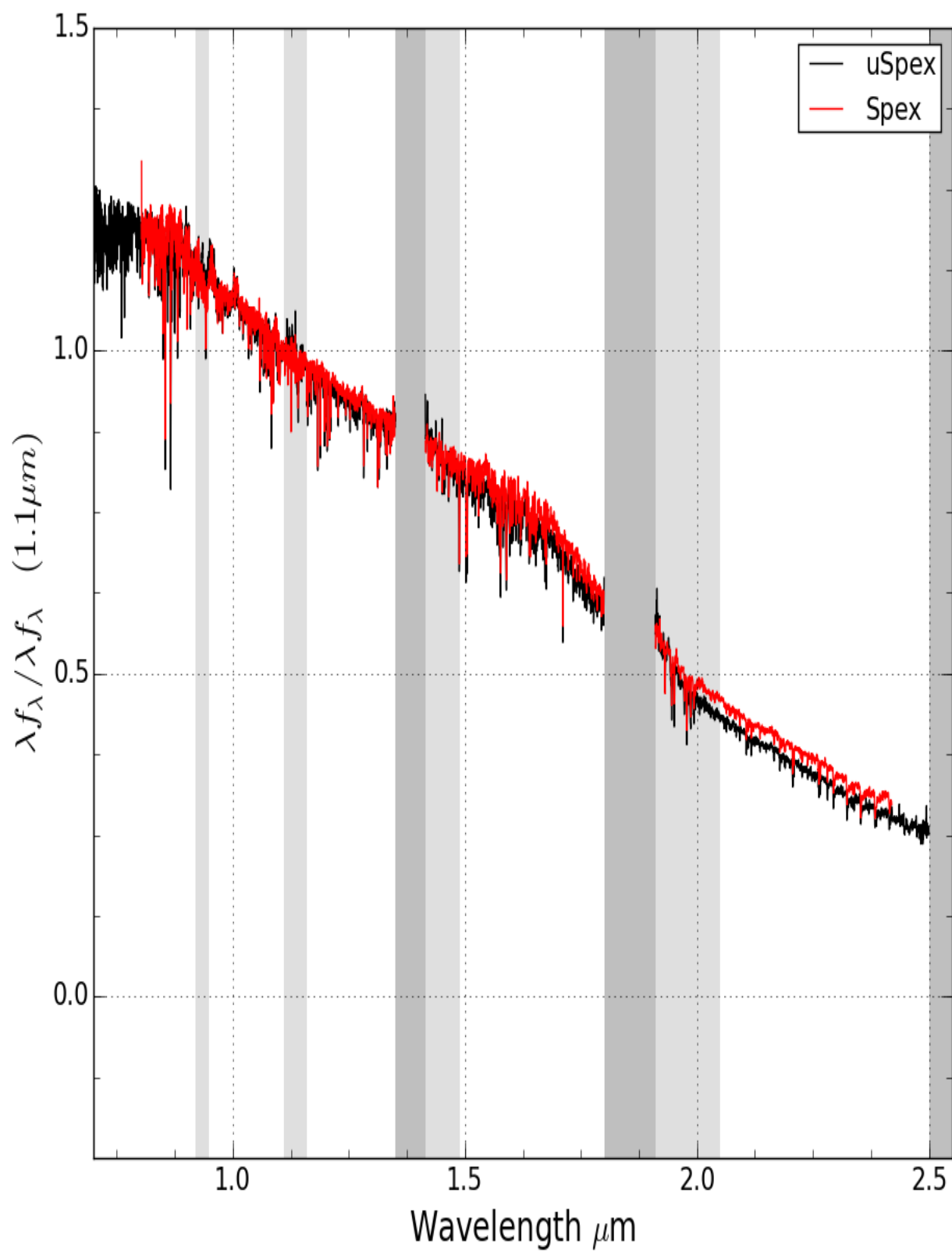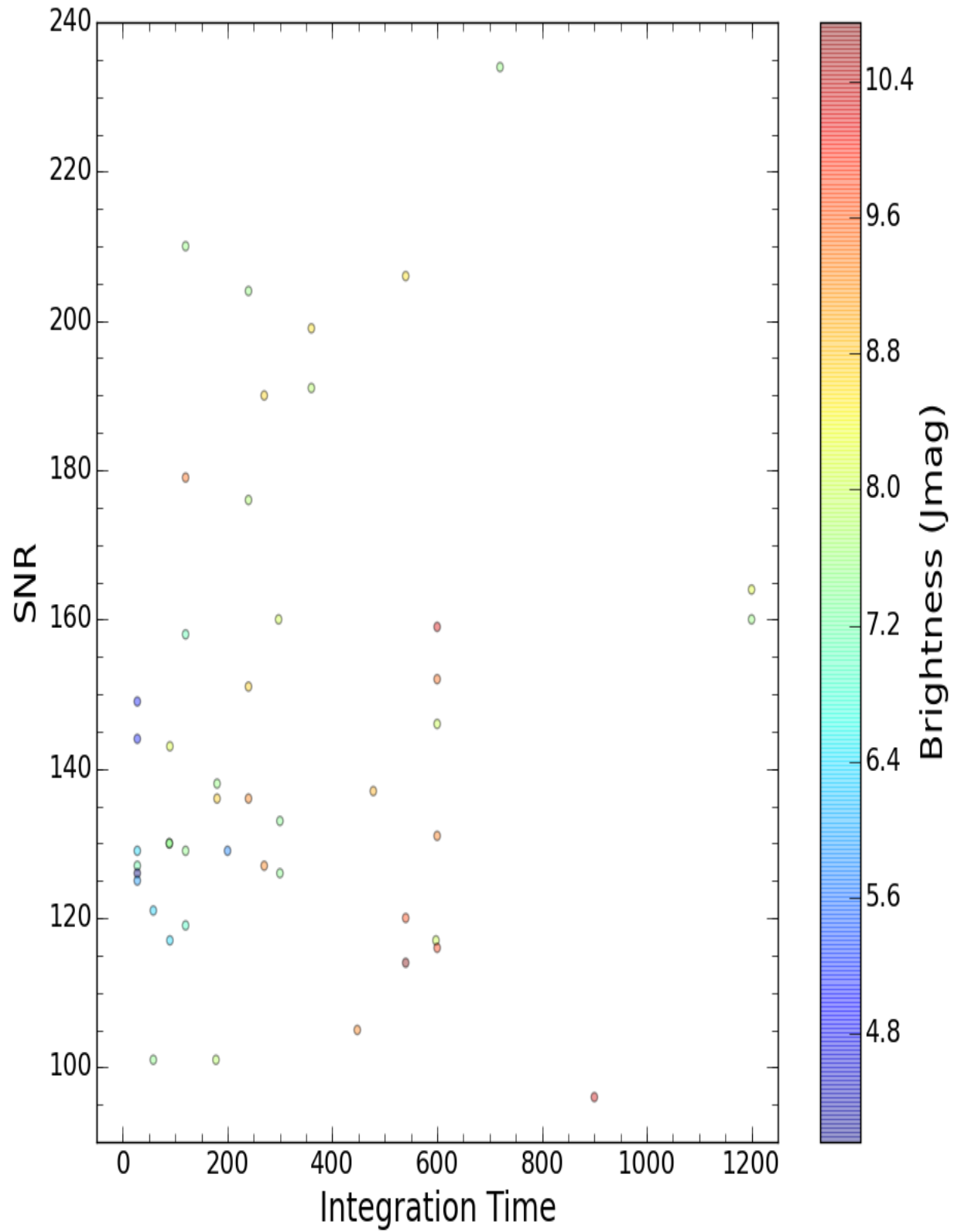For disks, it's a little simpler. You can just use Carpenter et al. (2006, 2009) and Luhman & Mamajek (2012).
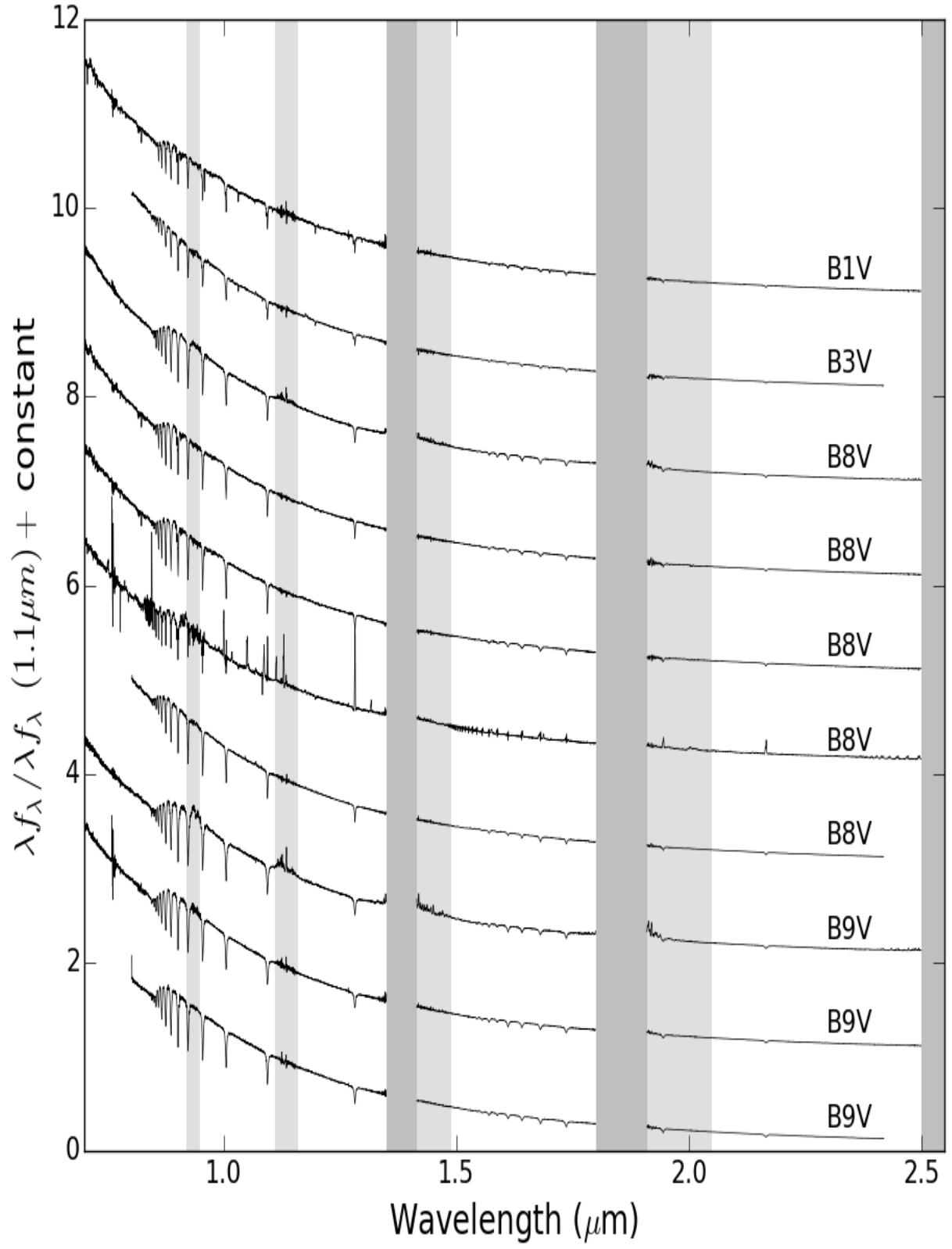
Spectral Composition of Library

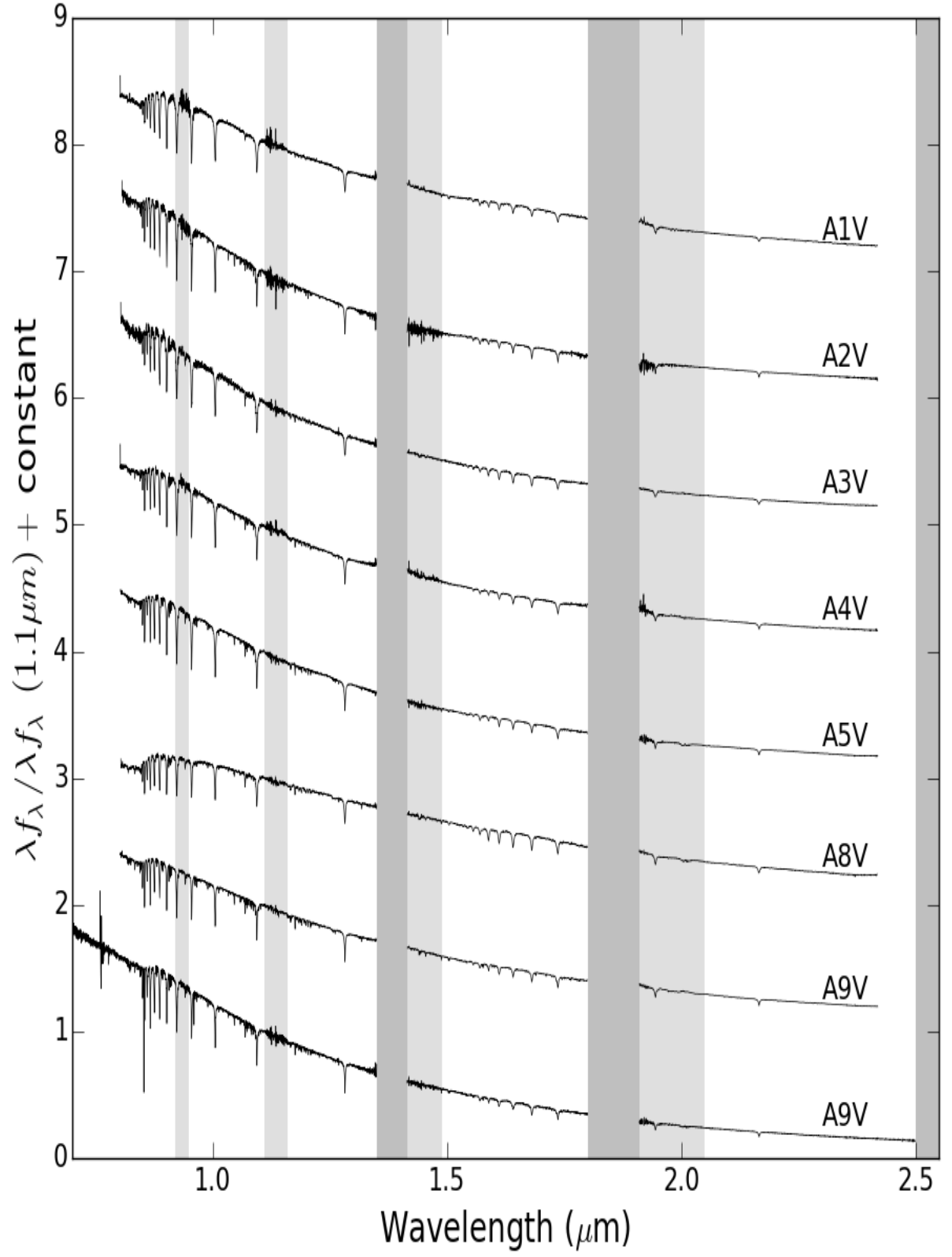Table 1: Listed here are observed targets with corresponding information.

| Object | RA | DEC | Lit. Spectral Type | UT Date | J (mag) | SNR | Total |
|---|---|---|---|---|---|---|---|
| HD 146266 | 16:16:23.32 | -25:03:49.1 | A1V | 7/18/2012 | 7.533 | 210 | |
| HD 143472 | 16:01:26.93 | -25:11:56.6 | A2V | 7/18/2012 | 7.074 | 158 | |
| HD 145468 | 16:11:52.96 | -22:32:42.1 | A3V | 6/29/2012 | 7.45 | 126 | |
| HD 142424 | 15:55:17.16 | -23:22:17.4 | A4V | 7/18/2012 | 7.54 | 138 | |
| HD 142097 | 15:53:21.87 | -21:58:20.6 | A5V | 7/12/2012 | 7.493 | 129 | |
| HD 146899 | 16:19:38.05 | -26:52:31.6 | A8V | 6/29/2012 | 8.569 | 206 | |
| HIP 73990 | 15:07:14.53 | -29:30:01.5 | A9V | 6/15/2015 | 7.499 | 130 | 8 |
| HD 147137 | 16:20:50.48 | -22:35:45.2 | A9V | 7/12/2012 | 8.032 | 146 | |
| HIP 78933 | 16:06:48.64 | -20:40:02.7 | B1V | 6/15/2015 | 4.16 | 126 | 2 |
| HD 144470 | 16:06:48.96 | -20:40:14.4 | B1V | 7/12/2012 | 4.16 | 44 | |
| HD 138485 | 15:32:55.67 | -16:51:16.5 | B3V | 7/12/2012 | 5.78 | 129 | |
| HD 147196 | 16:21:19.54 | -23:42:34.9 | B6/B7Vn | 7/12/2012 | 6.565 | 16 | |
| HIP 70753 | 14:28:10.35 | -29:29:26.1 | B8V | 6/15/2015 | 5.073 | 149 | 2 |
| HIP 77909 | 15:54:38.54 | -25:14:42.4 | B8V | 6/15/2015 | 5.925 | 125 | 2 |
| HIP 79031 | 16:07:51.15 | -24:27:47.7 | B8V | 6/15/2015 | 6.379 | 129 | 2 |
| HIP 78207 | 15:58:11.48 | -14:16:40.6 | B8V | 6/15/2015 | 5.098 | 144 | 2 |
| HD 144661 | 16:07:51.99 | -24:27:42.8 | B8V | 7/18/2012 | 6.379 | 117 | |
| HIP 76633 | 15:39:00.11 | -19:43:50.9 | B9V | 6/15/2015 | 7.476 | 101 | 5 |
| HIP 79599 | 16:14:28.97 | -21:06:20.4 | B9V | 6/15/2015 | 6.342 | 121 | 5 |
| HD 143567 | 16:01:55.60 | -21:58:50.4 | B9V | 7/18/2012 | 6.928 | 119 | |
| HD 137130 | 15:25:08.91 | -26:34:30.9 | F0V | 3/22/2012 | 7.566 | 160 | 1 |
| HIP 79369 | 16:11:55.19 | -21:06:10.4 | F1V | 6/15/2015 | 7.855 | 101 | 1 |
| HIP 82319 | 16:49:10.74 | -22:42:46.5 | F3V | 6/15/2015 | 8.05 | 117 | 5 |
| HD 146743 | 16:18:39.41 | -21:35:39.6 | F3V | 7/12/2012 | 7.838 | 191 | |
| HD 148153 | 16:27:12.68 | -27:11:27.2 | F5V | 7/12/2012 | 7.419 | 133 | |
| HIP 78977 | 16:07:17.56 | -22:03:39.8 | F7V | 6/29/2012 | 7.543 | 204 | |
| HIP 71982 | 14:43:19.42 | -10:35:13.5 | F8V | 6/15/2015 | 7.474 | 130 | 8 |
| HD 142113 | 15:53:21.17 | -19:23:58.8 | F8V | 7/12/2012 | 7.782 | 176 | |
| HIP 61412 | 12:35:00.73 | -26:42:46.3 | G0V | 6/15/2015 | 7.162 | 127 | 2 |
| HD 148040 | 16:26:29.32 | -27:41:17.0 | G0V | 3/22/2012 | 7.554 | 234 | |
| HD 133748 | 15:06:51.76 | -23:37:27.6 | G2V | 3/22/2012 | 8.251 | 164 | 1 |
| GSC 06793-00994 | 16:14:02.15 | -23:01:08.0 | G4V | 7/12/2012 | 9.375 | 131 | |
| HBC 649 | 16:34:09.09 | -15:48:01.4 | G5V | 6/15/2015 | 8.995 | 137 | 4 |
| GSC 06801-00186 (oldSpx) | 16:14:59.03 | -27:50:27.1 | K0IV(e) | 6/29/2012 | 9.334 | 136 | |
| GSC 06801-00186 | 16:14:59.30 | -27:50:17.9 | K0IV(e) | 6/15/2015 | 9.334 | 105 | 4 |
| GSC 06793-01406 | 16:16:17.80 | -23:39:51.3 | G7V | 6/29/2012 | 8.727 | 151 | |
| GSC 06213-00306AB | 16:13:18.19 | -22:12:52.3 | G9V | 6/29/2012 | 8.18 | 143 | |
| CD-25 11942 | 17:06:00.85 | -25:20:25.9 | K0V | 6/15/2015 | 8.099 | 160 | 2 |
| ScoPMS 214 | 16:29:48.69 | -21:52:17.2 | K0 / K2IV(e) | 7/12/2012 | 8.677 | 190 | |
| HD 141813 | 15:51:54.35 | -26:22:09.2 | K0 / K1III+ | 7/12/2012 | 8.232 | 30 | |
| HD 14311 | 15:58:57.31 | -13:10:14.3 | K0III | 7/12/2012 | 7.263 | 62 | |
| ScoPMS 44 | 16:11:08.86 | -19:04:51.8 | K2 / K2IV(e) | 7/12/2012 | 8.761 | 136 | |
| GSC 06793-00797 | 16:13:02.68 | -22:57:49.2 | K4V | 6/29/2012 | 9.322 | 127 | |

K0V

K0V

K0IV(e)

K0IV(e)

K2V

K4V

K5V

K6V

K9V

Wavelength ($\mu m$)

$\lambda f_\lambda / \lambda f_\lambda \, (1.1 \mu m) + \text{constant}$
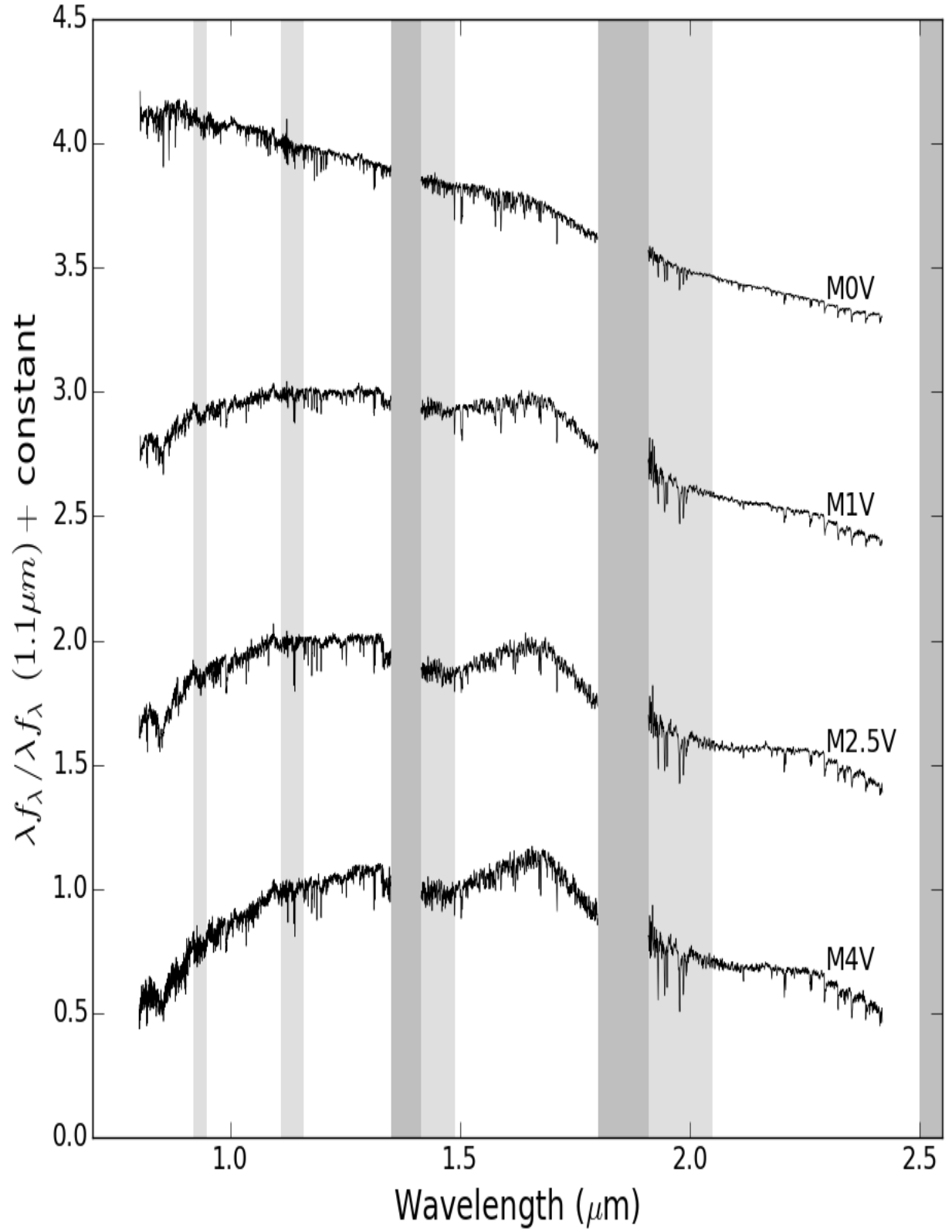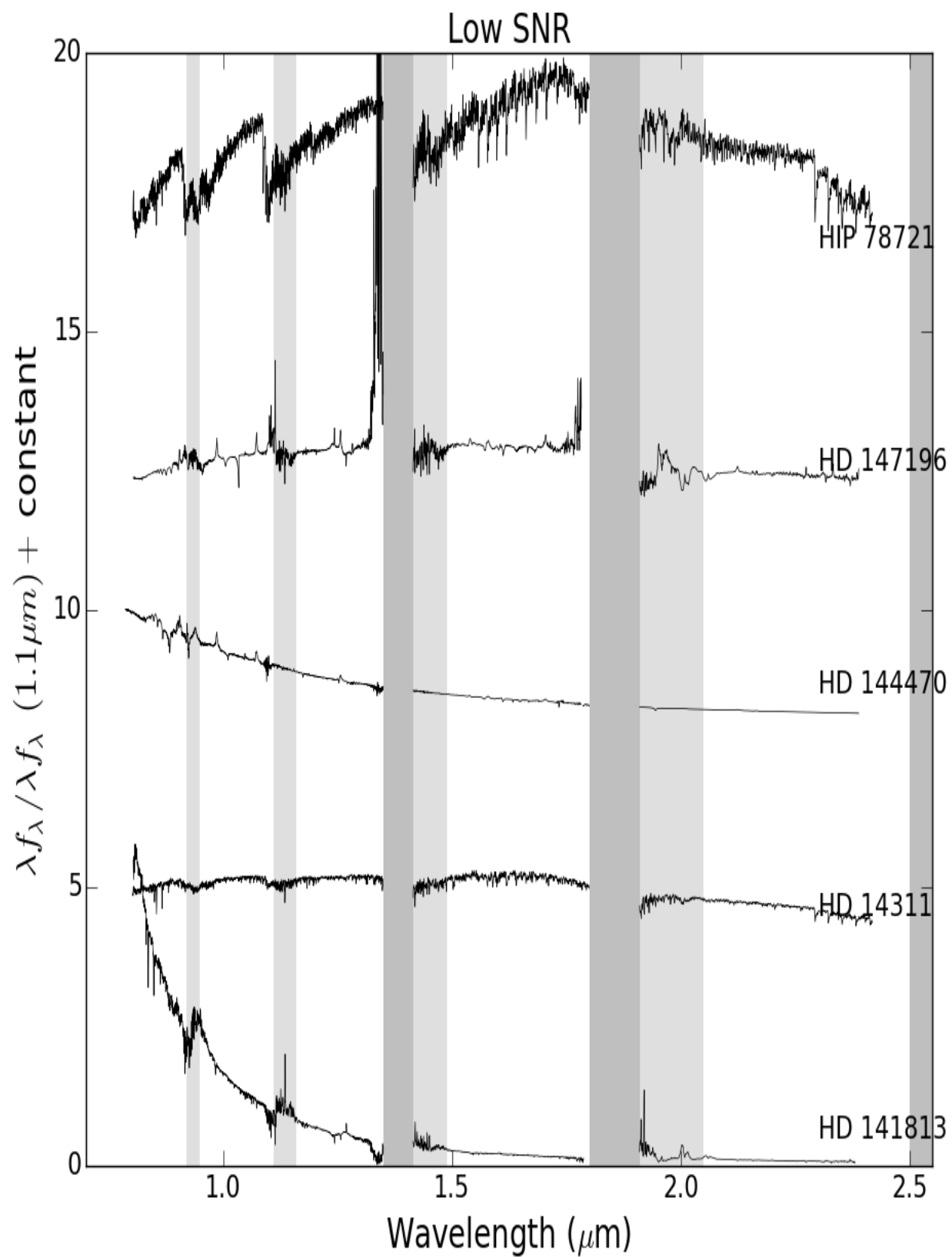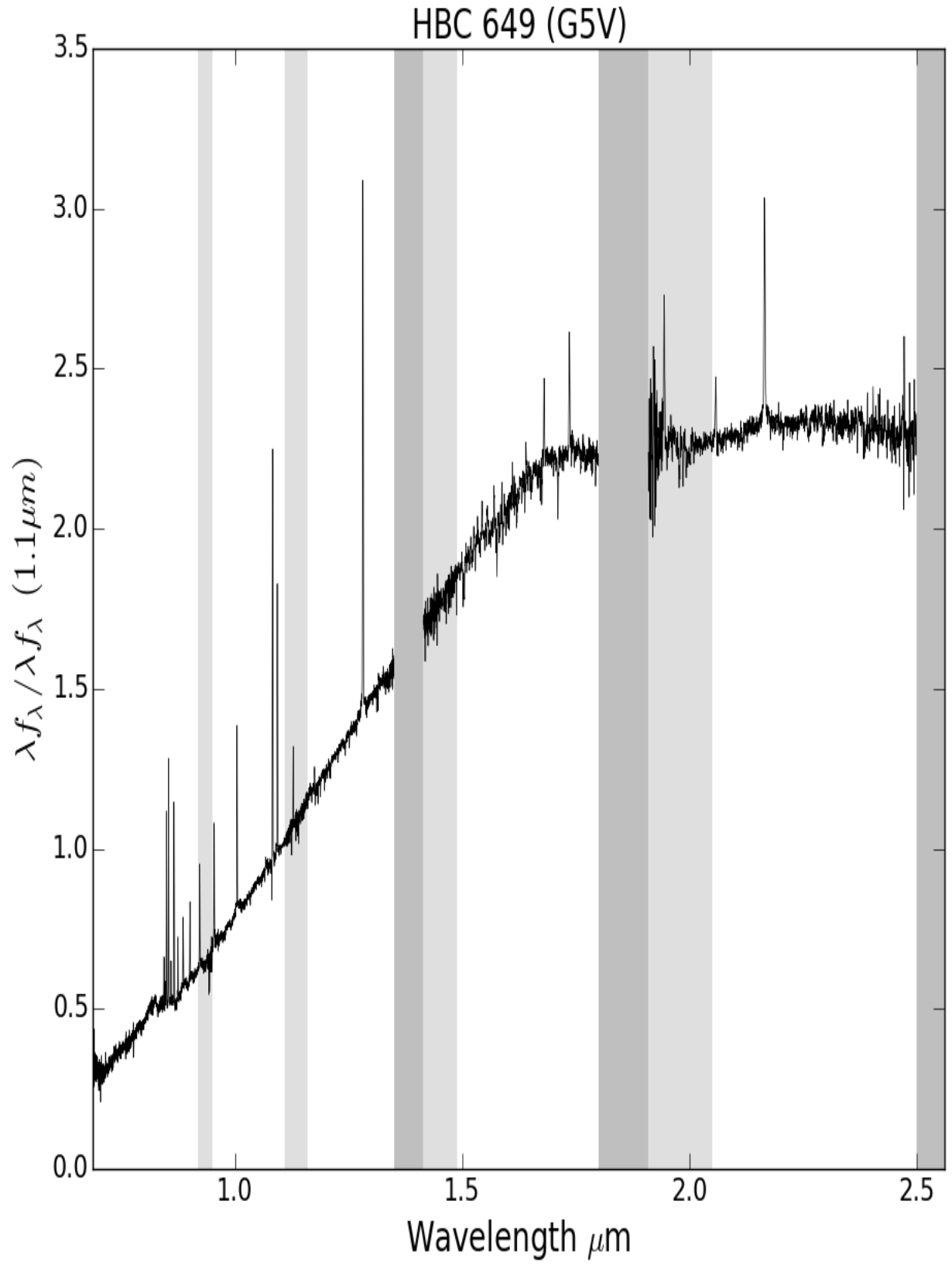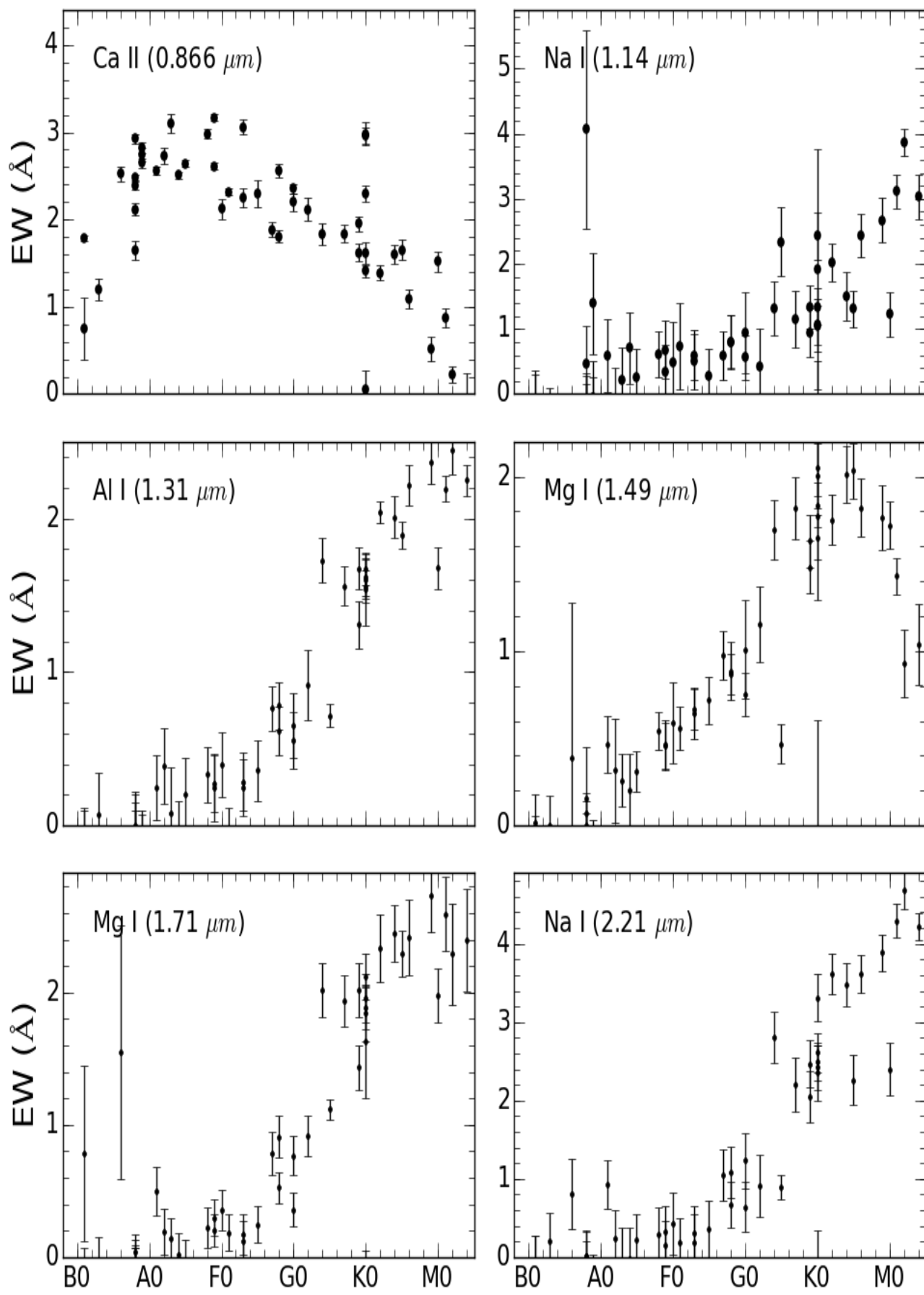
HBC 649 (G5V)
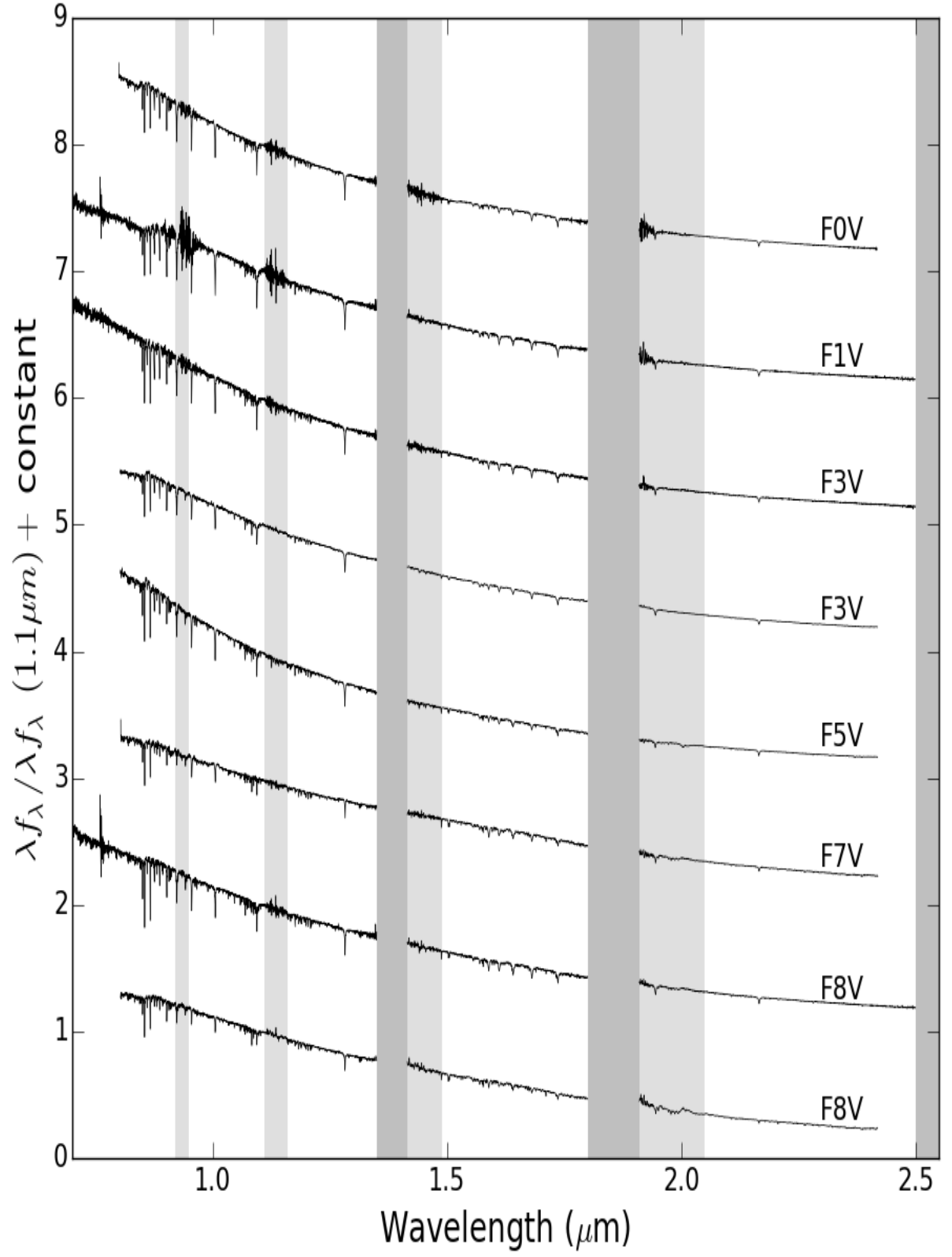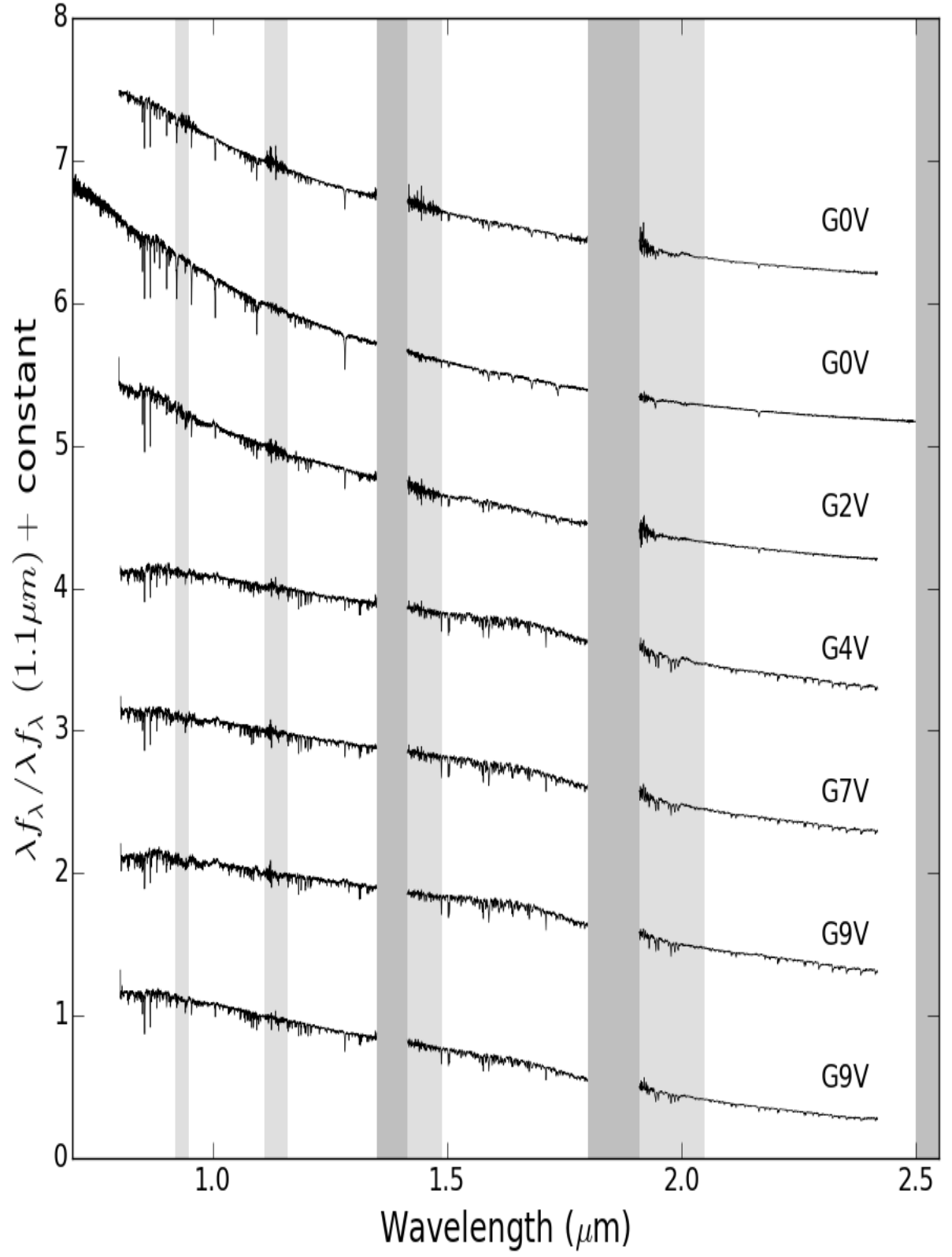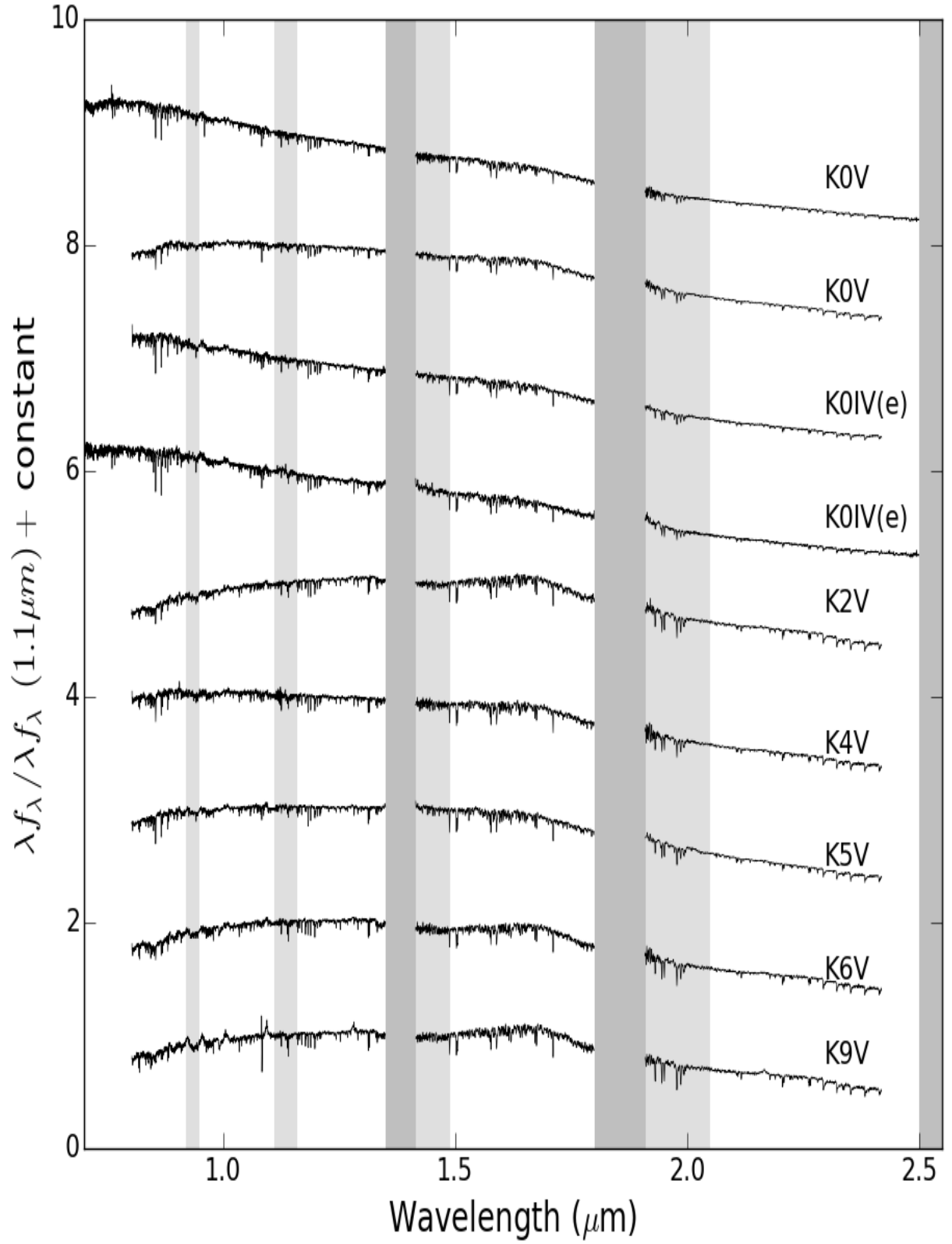
Table 3: EW values for spectral features listed in Table 2.

| Object | Spectral Type | Ca II (0.866$\mu m$) | Na I (1.14 $\mu m$) |
|---|---|---|---|
| HD 146266 | A1V | 2.56299927871±0.0505902823735 | 0.593124316048±0.55372199 |
| HD 143472 | A2V | 2.72620156086±0.0890465928405 | -0.124365182652±0.53092524 |
| HD 145468 | A3V | 3.09676507059±0.105335208586 | 0.219012800854±0.49378354 |
| HD 142424 | A4V | 2.50903380614±0.0418818508702 | 0.707624567334±0.54624929 |
| HD 142097 | A5V | 2.63724671857±0.0387032039504 | 0.249643364628±0.43915267 |
| HD 146899 | A8V | 2.98045841895±0.0563869594594 | 0.610106101858±0.35753207 |
| HIP 73990 | A9V | 3.16901597018±0.0343419109672 | 0.332887913546±0.41442923 |
| HD 147137 | A9V | 2.61193758312±0.0425581256529 | 0.674573918087±0.44666262 |
| HIP 78933 | B1V | 1.79060453404±0.0292219340768 | -0.225324048904±0.52465610 |
| HD 144470 | B1V | 0.748607183674±0.353534583215 | -0.189840080094±0.55912364 |
| HD 138485 | B3V | 1.20021713217±0.123249228036 | -0.459617243235±0.55869401 |
| HD 147196 | B6/B7Vn | 2.52213176697±0.0903438021126 | -2.6952099117±1.56138778 |
| HIP 70753 | B8V | 2.39216215594±0.0467874269198 | 0.458962358336±0.58055595 |
| HIP 77909 | B8V | 2.48348877896±0.0356986682689 | -0.163081246205±0.49287346 |
| HIP 79031 | B8V | 2.92313532374±0.0490276065772 | -0.302182483479±0.45369845 |
| HIP 78207 | B8V | 1.65203955311±0.108135748082 | 4.06821387941±1.52965998 |
| HD 144661 | B8V | 2.11294061833±0.0699405826986 | -0.30876422225±0.58216854 |
| HIP 76633 | B9V | 2.64639933676±0.0571975714836 | 1.38932051895±0.78741105 |
| HIP 79599 | B9V | 2.81912816636±0.0655007572171 | -0.0537110373563±0.56113468 |
| HD 143567 | B9V | 2.73921608292±0.0776068347864 | -0.346482479213±0.61236750 |
| HD 137130 | F0V | 2.1187101502±0.109996007908 | 0.478070933429±0.62315494 |
| HIP 79369 | F1V | 2.31937736651±0.0441335792305 | 0.736814084079±0.65470201 |
| HIP 82319 | F3V | 3.06056116029±0.0807534904999 | 0.596463524909±0.38397756 |
| HD 146743 | F3V | 2.25045438173±0.103381509043 | 0.498907766341±0.42552977 |
| HD 148153 | F5V | 2.29157107038±0.155742615121 | 0.269936653943±0.41998654 |
| HIP 78977 | F7V | 1.88231995991±0.0851137562302 | 0.591071362265±0.37699486 |
| HIP 71982 | F8V | 2.56060188894±0.0762131229772 | 0.798555225551±0.41701779 |
| HD 142113 | F8V | 1.80715735375±0.065280032777 | 0.807408187185±0.41124682 |
| HIP 61412 | G0V | 2.35262109221±0.0592524670013 | 0.563753159833±0.34277895 |
| HD 148040 | G0V | 2.20053757099±0.101688995449 | 0.945525631363±0.62576932 |
| HD 133748 | G2V | 2.11491753543±0.130076563777 | 0.434474969927±0.57501420 |
| GSC 06793-00994 | G4V | 1.82943169529±0.122746870859 | 1.30690699955±0.41515715 |
| HBC 649 | G5V | -11.1492957606±0.138296074012 | 2.34180866524±0.52749039 |
| GSC 06801-00186 (oldSpx) | K0IV(e) | 1.61984274243±0.120570710423 | 1.0591344803±0.39772763 |
| GSC 06801-00186 | K0IV(e) | 2.95767211472±0.089655798648 | 2.4310123804±0.35865474 |
| GSC 06793-01406 | G7V | 1.83580456818±0.0985098972086 | 1.15935055549±0.43504243 |
| GSC 06213-00306AB | G9V | 1.62311949533±0.100699089538 | 1.33688888145±0.33450816 |
| CD-25 11942 | K0V | 2.30203721938±0.0933113714974 | 1.05295210041±0.29715866 |
| ScoPMS 214 | K0 / K2IV(e) | 1.40960995147±0.0646030261218 | 1.34696384811±0.28520075 |
| HD 141813 | K0 / K1III+ | 0.0522366059582±0.215325641091 | 1.90968185145±1.84440442 |
| HD 14311 | K0III | 2.98372410744±0.130486483868 | -0.235621959504±0.74817149 |
| ScoPMS 44 | K2 / K2IV(e) | 1.3889969003±0.0833266847196 | 2.02571434786±0.29050609 |
| GSC 06793-00797 | K4V | 1.60031113319±0.109051356026 | 1.5075712139±0.37319813 |